A novel pulsed STED microscopy method using FastFLIM and the phasor plots

Yuansheng Sun[1,*], Giorgio Tortarolo[2,*], Kai-Wen Teng[3], Yuji Ishitsuka[3], Ulas C. Coskun[1], Shih-Chu Jeff Liao[1], Alberto Diaspro[4], Giuseppe Vicidomini[2], Paul R. Selvin[3], Beniamino Barbieri[1]

[1]ISS, Inc., 1602 Newton Drive, Champaign, IL 61822, USA
[2]Molecular Microscopy and Spectroscopy, Nanophysics, Istituto Italiano di Tecnologia, Via Morego 30, Genoa 16163, Italy
[3]Department of Physics, University of Illinois at Urbana-Champaign, 1110 West Green Street, Urbana IL 61801, USA
[4]Nanoscopy, Nanophysics, Istituto Italiano di Tecnologia, Via Morego 30, Genoa 16163, Italy

[*]Equal contribution and authors to whom correspondence should be addressed:
Yuansheng Sun, Yuansheng.Sun@iss.com. Giorgio Tortarolo, giorgio.tortarolo@iit.it.

ABSTRACT

Stimulated emission depletion (STED) microscopy is a powerful super-resolution microscopy technique that enables observation of macromolecular complexes and sub-cellular structures with spatial resolution below the diffraction limit. The spatial resolution of STED is limited by power of the depletion laser at the specimen plane. Higher depletion laser power will improve resolution, but at the cost of increased photo-bleaching, photo-toxicity, and anti-stoke emission background. This degrades the signal-to-noise ratio, and can significantly limit STED applications in living specimens. Here, we present an efficient multi-color STED microscopy method based on the digital frequency domain fluorescence lifetime imaging (FastFLIM) and the phasor plots. Our approach utilizes a combination of pulsed excitation and pulsed depletion lasers to record the time-resolved photons by FastFLIM. We demonstrate that the resolution is improved without increasing the depletion laser power by digital separation of the depleted species from the partially depleted species based on their different decay kinetics. We show the utility of this novel STED method applied in both fixed and live cellular samples, and also show its application to fluorescence lifetime correlation spectroscopy (FLCS) measurements. By combining fluorophores with different fluorescence lifetimes, we simultaneously record two-color STED images of cells labeled with Atto655 and Alexa647 in a single scan by using a single pair of excitation and depletion lasers. This novel approach shortens the data acquisition time while minimizing the photo-toxicity caused when using two separate depletion lasers.

1. INTRODUCTION

Ernst Abbe determined that the fundamental spatial resolution of the visible light microscope is limited by the diffraction of light to approximately 200 nm when using a high numerical aperture objective lens. Recently, several super-resolution fluorescence microcopy techniques including STimulated Emission Depletion (STED) microscopy [1-3], Photoactivated localization microscopy (PALM) [4-7], and STochastic Optical Reconstruction Microscopy (STORM) [8-11] have been developed that circumvent the diffraction limit to achieve resolutions of below 20 nanometers. Each of these super-resolution fluorescence microscopy techniques achieves sub-diffraction resolution by manipulating the transition between bright (on) and dark (off) states of the fluorescent molecules. At a particular time, for any diffraction-limited volume under observation, only the molecules within a much smaller sub-diffraction volume are tuned "on" whilst the rest neighboring molecules are "off".

In STED microscopy, this transition is achieved by using two lasers: an excitation laser turns "on" the fluorophores causing the transition from the ground state to the excited-state, while the second depletion laser turns a subset of fluorophores "off" from its excited-state back to the ground state by means of stimulated emission. This approach

Multiphoton Microscopy in the Biomedical Sciences XVII, edited by Ammasi Periasamy, Peter T. C. So, Karsten König, Xiaoliang S. Xie, Proc. of SPIE Vol. 10069, 100691C

generates a sub-diffraction volume by engineering a donut-shaped point spread function (PSF) of the depletion beam relative to the Gaussian-shaped PSF of the excitation beam. The depletion PSF has a zero-intensity spot at the center of the excitation PSF and strong intensity at the periphery of the excitation PSF. Thus, the STED microscope constrains the resolution to the zero-intensity spot within the donut-shaped PSF, and its full-width half maximum (FWHM) can be estimated by a modified Abbe's equation: $r = \lambda/\left(2NA\sqrt{1 + (I_{STED}/I_{Sat})}\right)$, where λ denotes the light wavelength; NA is the objective numerical aperture; I_{STED} is the donut crest intensity of the applied depletion beam and I_{Sat} is the saturation intensity of the STED beam.

The STED approach to switching the on-off states of the fluorescent molecules is fundamentally different from that used by single-molecule-localization (SML) techniques such as PALM or STORM. In a typical PALM/STORM experiment, all fluorescent molecules are initially in the dark state. A series of hundreds to thousands of imaging cycles is used to turn a subset fluorophores on and off. This series of cycles is then used to reconstruct a super-resolution image. This approach uses low power excitation to turn on only a few random spatially distinct fluorophores with each cycle. The positions of the fluorescence emission photons are recorded, and the fluorophores are switched back to the dark state permanently prior to the next imaging cycle. The number of photons (N) determines the localization precision; thus in comparison to STED, the PALM/STORM resolution is estimated by $r = \lambda/\left(2NA\sqrt{N}\right)$. Because of the random nature of the activation process in space, the performance of PALM or STORM critically depends on the labeling density, and requires many imaging cycles to permit the reconstruction of a single super-resolution image. Although the detection is wide-field, the necessity for many imaging cycles to reconstruct an image significantly limits the imaging speed. In contrast, STED precisely controls switching on and off the fluorescent molecules in space by engineering the depletion PSF. Thus, STED can tolerate a much wider range of labeling densities, and a super-resolution image is typically obtained by a single raster scan in the laser scanning confocal system.

A critical factor for the STED microscopy is the depletion efficiency, mainly affected by "I_{STED}/I_{Sat}" - the STED laser intensity relative to the saturation level. Effective sub-diffraction resolution is only achieved when $I_{STED} >> I_{Sat}$. The STED saturation intensity, at which half of the fluorescence is suppressed by STED, is given by $I_{Sat} = h\upsilon/(\sigma\tau)$, where $h\upsilon$ is the photon energy; σ is stimulated emission cross section; τ is the fluorescence excited state lifetime [12,13]. The STED laser intensity required to achieve sub-diffraction resolution is on the order of 0.1 ~ 1 GW/cm^2 [12]. However, laser powers in this range can introduce photo-toxicity in live specimens, especially when using a continuous-wave (CW) beam. This problem is overcome by using pulsed excitation with the CW STED laser and time-gating the detection, such that the photons are only collected after a certain delay following the excitation pulse (typically the fluorescence lifetime) [12]. However, this method degrades the signal-to-noise ratio because significant numbers of "good" photons emanating from the center of the sub-diffraction volume are discarded.

The Separation of Photons by LIfetime Tuning (SPLIT) method is an improvement from cwSTED - it takes time-resolved measurements and uses the phasor plot approach to separate the wanted photons emitted in the center region from the unwanted photons resulting from incomplete depletion in the donut region and from the anti-Stokes emission background generated by the STED beam [14]. Unlike the gating method, the SPLIT method analyzes different decay dynamics of the wanted vs. the unwanted photon species using the phasor plot approach, and identifies the photons emitted from the center of zero depletion without sacrificing the signal-to-noise ratio.

Instead of using the cw laser for STED, more efficient depletion can be achieved by applying both pulsed excitation and pulsed depletion (pulsed STED - pSTED), which was actually the setup used in the very first STED microscopy experiment [15]. The pSTED method synchronizes the arrival times of both excitation and depletion laser pulses at the specimen plane, such that the molecules are first driven by the excitation pulse to the excited state and then immediately de-excited by the STED pulse. It is important to recognize the trade-off between photo-bleaching and resolution that is determined by the width of the STED pulse. For the same average intensity, a longer pulse will have lower peak intensity and less photo-bleaching. However, this also results in a lower depletion efficiency leading to less effective resolution [13,16-18]. A recent study comparing the 200-ps vs. 600-ps STED pulses demonstrated that the photo-bleaching was reduced by using the longer STED pulse, while the effective resolution was maintained by using the time-gating detection [18].

In this paper, we describe a novel pSTED method to acquire the time-resolved STED images using FastFLIM, a data acquisition unit developed based on the digital frequency domain (DFD) technique [19]. Compared to the time

correlated single photon counting (TCSPC) technique, FastFLIM provides a wider linear dynamic range of counting photons, since it has nearly no dead time. We show the results obtained by applying the FastFLIM-pSTED method to several different samples, including solutions, and fixed or live cells. The capabilities for various STED measurements and fluorescence lifetime correlation spectroscopy (FLCS) are demonstrated, and we show how the phasor plot approach is used to sharpen the time-resolved pSTED image acquired by FastFLIM. Finally, we propose a new way of using a single excitation/depletion-laser combination to acquire the dual-label STED images with FastFLIM.

2. MATERIALS AND METHODS

2.1 The pSTED schematic

Figure 1 shows the schematic of the pSTED setup, implemented on an ISS Alba confocal / multiphoton laser scanning microscopy system (www.iss.com/microscopy/instruments/alba.html). It is coupled to a Nikon TE2000 microscope equipped with a Nikon Plan APO λ 60X/1.4NA oil objective lens. Galvo mirrors are used for the XY scan of a sample, and the optical sectioning is performed by mounting the objective lens on a Piezo-Z device (MadCity Labs). The scanning and piezo devices are synchronized to the data acquisition unit(s) for both the SPC-150 board (Becker Hickl) for TCSPC measurements and FastFLIM by ISS for DFD measurements. The typical detectors used by Alba (up to 4 channels) are GaAsP (H7422p, by Hamamatsu) or Hybrid (R10467, by Hamamatsu) photomultiplier tubes (PMTs) or single photon counting module (SPCM, by Excelitas) avalanche photodiodes (APDs); this 2-channel Alba system uses the SPCM-ARQH-15 APD detector in channel 1 and the H7422p-40 PMT detector in channel 2. Both data acquisition and analysis are performed using the ISS VistaVision 64-bit software.

A 640-nm picosecond pulsed diode laser (Becker Hickl, BDL-SMN-640, ~120 ps pulse width) is used as excitation beam. A 775-nm sub-nanosecond pulsed fiber laser (OneFive, Katana 775, ~600 ps pulse width) is used as STED beam. The two lasers were synchronized by either (a) using the depletion laser at the 40 MHz repetition rate (master) to trigger the excitation laser (slave); or (b) using the excitation laser at the 50 MHz repetition rate (master) to trigger the depletion laser (slave). Both lasers are synchronized to both the FastFLIM and the TCSPC data acquisition units for the time-resolved STED measurements. The 640-nm excitation laser is mounted on the ISS 3-diode laser launcher for its intensity control, and then delivered to the Alba system via a single mode polarization maintained fiber (QiOptics). The 775-nm STED laser intensity is controlled by the ISS intensity control unit containing a motorized rotating halfwave plate and a fixed Glan-Thompson polarizer. Before entering the Alba system, the STED laser beam first passes the optical delay line (ODL) for the fine tuning (picoseconds) of the time delay between the excitation and STED pulses on the specimen plane; it is delivered via a single mode polarization maintained fiber (Thorlabs) to the STED beam condition module (SBCM) for generating the donut-shape beam of circular polarization – both ODL and SBCM were custom made by ISS.

In Alba, the excitation and the STED beams are first combined by a 670 long-pass dichroic (D1, Semrock), and the main dichroic (D2, custom made by Chroma) passes both laser beams and reflects the de-scanned emission light. For STED measurements in channel 1, the emission light is filtered by both a OD 8 720-nm short-pass NIR light blocking filter (Chroma), and a 679/41-nm band-pass emission filter (Semrock). A motorized confocal pinhole tunable from ~20 µm continuously to 1 mm is placed before each detector; the pinhole in channel 1 was set to be 60 µm (~ 1 Airy Unit) for STED measurements.

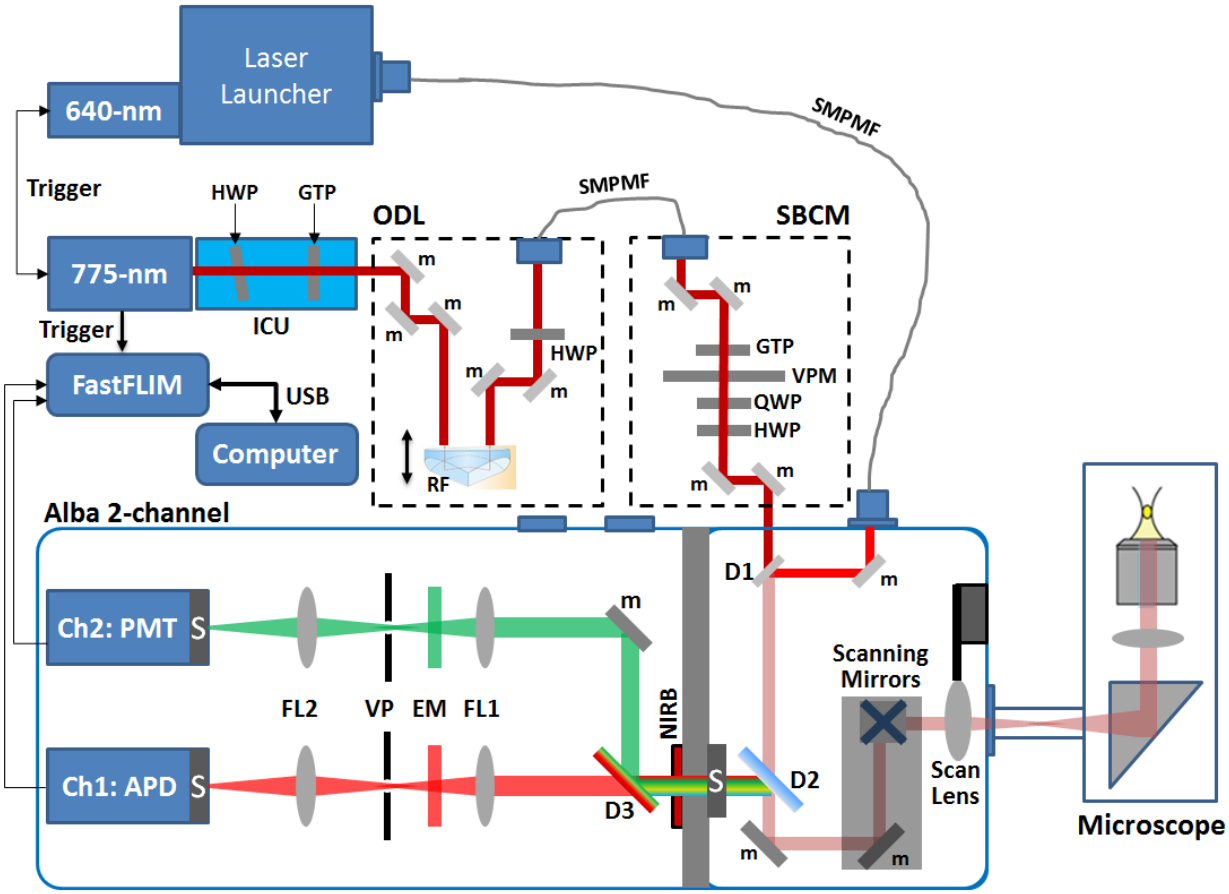

Figure 1: The Schematic of the pulsed FastFLIM-STED. (ICU: intensity control unit; HWP: halfwave plate; GTP: Glan–Thompson polarizer; ODL: optical delay line; RF: Retroreflector; SMPMF: single mode polarization maintained fiber; SBCM: STED beam conditioning module; QWP: quarter wave plate; VPM: vortex phase mask; m: mirror; D (D1, D2, D3): dichroic; S: shutter; NIRB: NIR light blocking filter; FL (FL1, FL2): focusing lens; EM: Emission Filter; VP: Variable Pinhole).

2.2 FastFLIM for the time-resolved pSTED image acquisition

FastFLIM (www.iss.com/microscopy/components/FastFLIM.html) records the photon counts in a number of cross-correlation phase bins that are represented as phase histograms used for the DFD FLIM data analysis [19]. FastFLIM has nearly no dead time for time-resolved data acquisition, leaving the limitation only to the detector itself. In contrast, the classical high tempo-resolution TCSPC devices typically have a dead time of 100~150 ns, and a non-linear effect of photon counting is typically seen at ~10% of the reciprocal of the dead time [20], limiting the dynamic range for quantitative measurements, especially for the typically used 40~80 MHz repetition rate lasers. Figure 2 shows a comparison of the photon counting capability between FastFLIM and the SPC-150 TCSPC card based on the same experimental conditions. For TCSPC, the counting loss is seen at the rate of ~ 1 million counts per second, expected for the SPC-150 dead time of 100 ns. Therefore, FastFLIM is capable of covering the whole dynamic range provided by the detector (H7422p-40).

FastFLIM is designed and implemented using field programmable gate array (FPGA), and is easily programmable to fit into different applications; it provides four independent data input channels, allowing data acquisition from four detectors simultaneously. FastFLIM provides a nice feature for the STED microscopy imaging – on one hand it acquires the DFD data to analyze the complicated decay kinetics and estimate a wide range of lifetimes (tens of picoseconds to hundreds of microseconds); on the other hand it uses the full potential of the detector for the photon counting.

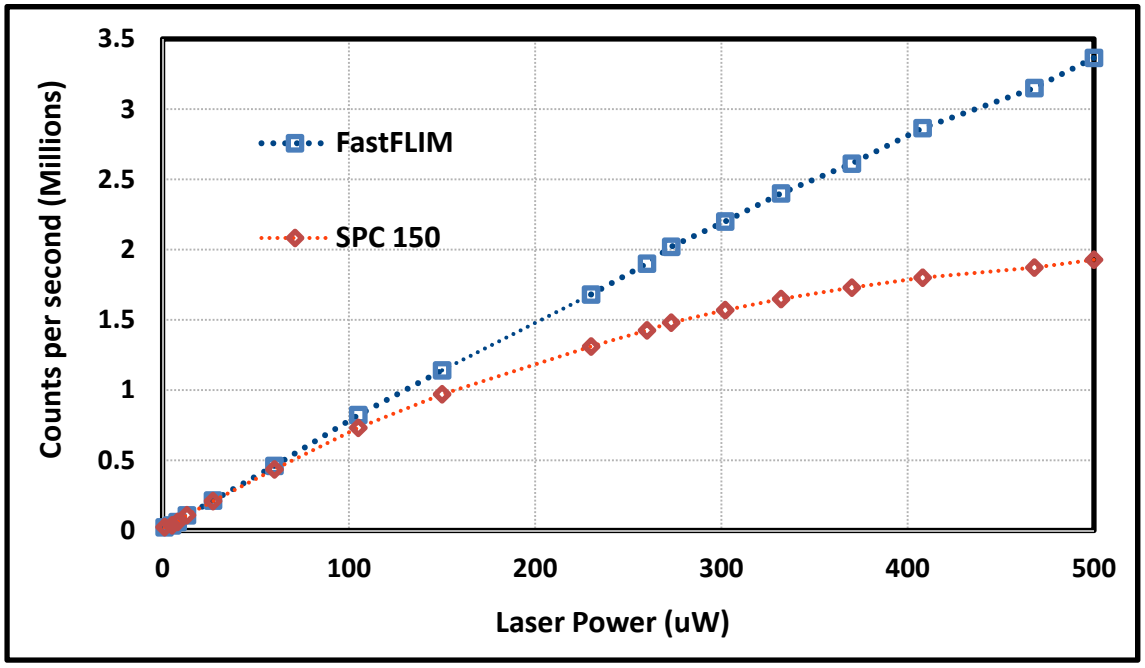

Figure 2: Comparison of the photon counting capability between FastFLIM and SPC-150.

2.3 The phasor plot for the time-resolved pSTED image processing and analysis

The phasor plot [21,22], also known as the polar plot [23] or the AB plot [24,25] is a powerful method for FLIM data analysis. It transforms the phase (ϕ) and the modulation (m) measurements in the frequency domain to the phasor space (G, S), as $G_\omega = m_\omega \cdot \cos(\phi_\omega)$ and $S_\omega = m_\omega \cdot \sin(\phi_\omega)$, where ω is the modulation frequency. The raw FLIM measurements from each pixel are directly located on a 2D phasor plot. For a single-lifetime species, the phase lifetime ($\tau_\phi = (\tan\phi)/\omega$) and the modulation lifetime ($\tau_m = (1\text{-}m^2)^{1/2}/(m\omega)$) are equal, from which a relationship between the G and S coordinates is derived as "$S^2 + (G\text{-}0.5)^2 = 0.25$". This relationship is represented as a semicircle curve centering at (G=0.5, S=0) with a radius of 0.5 on the phasor plot. The semicircle curve indicates the lifetime trajectory with decreasing lifetime from left to right, where (1, 0) indicates lifetimes near zero to (0, 0) being infinite lifetime. Since no fitting is involved, the phasor plot approach is independent of any underlying physical model. By plotting raw data in the phasor plot, one can distinguish between single- and multi-component lifetimes, identify the lifetime value of a single-lifetime species, and visualize and quantify the relative lifetime changes between complex lifetime distributions. More importantly, many data distributions measured from different samples can be directly compared in a same phasor plot [26,27].

The phasor plot approach provides a linear way of analyzing a complex mixture (G_ω, S_ω) composed of multiple (e.g. N) species, each of which is represented by a unique phasor ($G_{\omega,i}$, $S_{\omega,i}$) and can behave as a single-exponential (on the semicircle) or multi-exponential (inside the semicircle) decay kinetics:

$$G_\omega = \sum_{i=0}^{N}(f_i \cdot G_{\omega,i})\ ;\ S_\omega = \sum_{i=0}^{N}(f_i \cdot S_{\omega,i})\ ;\ \sum_{i=0}^{N}(f_i) = 1\ ;$$

where f_i denotes the contribution of the i^{th} species to the mixture. When the phasor signature of each species ($G_{\omega,i}$, $S_{\omega,i}$) is known and given the measurements of enough harmonics (ω), decomposing the mixture will yield the contribution of each species (f_i). Figure 3 shows how the phasor plot is used to decompose a mixture of Rhodamine 110 and Rhodamine B in solution using the phasor signatures that are obtained by measuring the individual samples separately.

The same concept of decomposing different species using the phasor plot approach can also be applied to improve the STED resolution described by the SPLIT method [14]. The time-resolved STED image encodes the information of different decay kinetics resulting from that molecules may interact with the excitation only or both the excitation and the

depletion. Decoding (Decomposing) different decay kinetics using the phasor plot approach can separate the photons of a specific decay kinetic (i.e. by the excitation only) from others, yielding an increased resolution. This encoding / decoding process requires the time-resolved data acquisition for STED, which can be done either by TCSPC or DFD (FastFLIM). Here, we show that this is achieved more simply by FastFLIM and the phasor plot approach, which uses the frequency-domain data. It is critical to accurately determine the phasor signature of each of the decay kinetics, which are used in the decomposition process to obtain the contribution of each species (f_i), as described above. Last, the raw STED steady-state signal (I) is decomposed into N components by ($f_i \cdot I$), producing N steady-state intensity images for the N signatures of the decay kinetics. The image representing the excitation-only decay kinetics at the donut center should give a better resolution than the raw STED image, although the improvement depends on the signal-to-noise ratio.

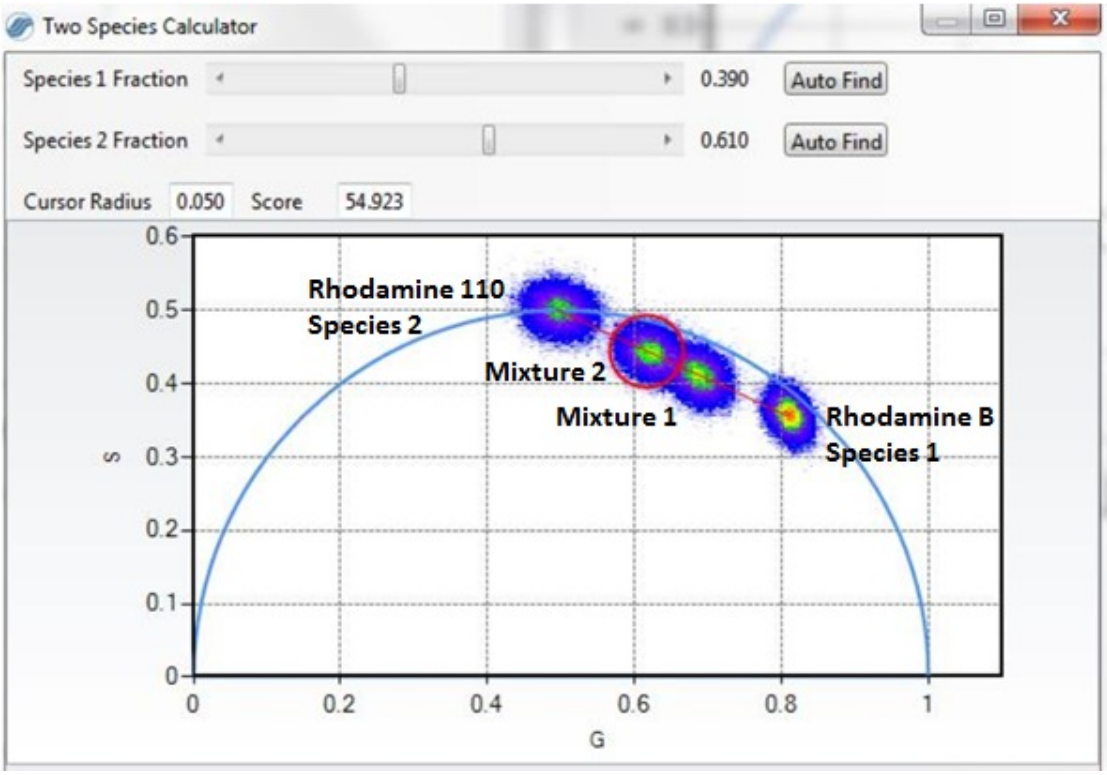

Figure 3: Decomposing two species of different lifetimes on the phasor plot – in mixture 2, 39% is Rhodamine B and the rest is Rhodamine 110.

2.4 Sample preparations

Gold beads of 80-nm diameter (Sigma-Aldrich) were diluted in water by 1: 200 (v/v) for a sparse sample. The diluted solution was dropped onto a poly-L-lysine (Sigma-Aldrich) coated glass coverslip. After 5 min the coverglass was rinsed with water, and dried under compressed air, and mounted using the immersion oil from Nikon. A diluted solution (1: 1000 in water,v/v) of Crimson fluorescent beads of 60-nm diameter (FluoSpheres Red and Crimson, Thermo Fisher) was used to prepare the fluorescent beads sample, using the same protocol, but with Mounting Medium from Invitrogen.

HeLa cells were transfected with plasmid DNA encoding GFP-ActA-Halotag [28] (ActA binds to the outer mitochondrial membrane) overnight using Lipofectamine 2000 (Life Technologies) following manufacturer's protocol. The cells were fixed using 4% paraformaldehyde (Fisher Scientific), and permeabilized with 0.2% Triton-X 100 (Sigma). The cells were then labeled with ATTO647-GBP (GFP-Booster, Chromotek) in the presence of 3% bovine serum albumin (BSA) in PBS. After labeling the cells were fixed using 4% paraformaldehyde for 15 minutes. For labeling the mitochondria of living cells with Alexa647 chloroalkane (Halotag ligand), transfected HeLa cells expressing GFP-ActA-Halotag were permeabilized and labeled as described earlier [29]. The HeLa cells were treated with 100 U/mL of

Streptolysin O (SLO) for 10 min, followed by 5 min of incubation time with chloroalkane Alexa647 on ice, and the permeabilized cells were recovered with DMEM 10% FBS supplemented with ATP, GTP, and glucose.

All experimental procedures involving animals were approved by the Institutional Animal Care and Use Committee at the University of Illinois Urbana-Champaign. Primary hippocampal and glia cultures were prepared from E 18.5 Sprague–Dawley rat embryos as described previously [30] with the following modifications. Neurons were dissociated in 3 mg/mL protease (Sigma, P4032) and plated on 25 mm coverslips (1.8 x 10^5 cells/coverslip) coated with 0.1 mg/mL poly-D-Lysine (Sigma-Aldrich) suspended in the plating medium (MEM (Sigma, 51412C) with 10% FBS, 25 mM glucose, 1 mM sodium pyruvate, 25 µM L-glutamine, 50 U/mL penicillin and 50 U/mL streptomycin). After 4 hours, the medium was exchanged to maintenance medium (Neurobasal medium (ThermoFisher Scientific) with B-27 supplement, 0.5 mM L-glutamine, 50 U/mL penicillin and 50 U/mL streptomycin) and continued culturing at 37°C with 5% CO_2. Between 3-5 days *in* vitro (DIV) cytosine arabinoside was added to the final concentration of 1 mM to suppress the glial proliferation. Fresh maintenance medium was fed every 3-4 days. On 11-13 DIV, neurons were co-transfected with plasmids with Homer1-mGeos-M (0.8 µg/coverslip), GluR2-AP (0.8 µg/coverslip), BirA-ER (0.8 µg/coverslip) and GPI-RFP (0.8 µg/coverslip) using Lipofectamine 2000 diluted in Neurobasal medium. Transfected cells were grown for additional 24-48 hours.

Glia and neurons were labeled as follows. Before labeling, all coverslips were first transferred to warm imaging buffer (25 mM Hepes, pH 7.3 with 125 mM NaCl, 2.5 mM KCl, 2 mM $CaCl_2$, 1 mM $MgCl_2$ and 33 mM glucose). For actin labeling, glia cells were incubated with 2 mM SiR-Actin (Cytoskeleton, Inc.) dissolved in the imaging buffer for 10 min at 37 ^oC. For dual labeling of membrane and AMPA receptor, neurons expressing GPI-RFP, biotinylated GluR2 and Homer1-mGeos-M were first incubated in 3 nM streptavidin-Atto647N diluted in imaging buffer with 0.6% BSA for 5 min. Subsequently, cells were incubated in 50 nM RBP-Atto655 (RFP-booster, Chromotek) diluted in imaging buffer with 0.6% BSA for 10 min. Cells were washed with imaging buffer with 0.6% BSA between steps. After labeling steps, all cells were fixed using 4% paraformaldehyde for 15 min at the room temperature.

3. RESULTS AND DISCUSSIONS

3.1 The spatial and temporal alignments for the pSTED

The gold nanoparticles were used for verifying the spatial and temporal alignments between the excitation and the STED laser beams. The Gaussian (excitation) and donut (STED) PSFs (Figure 4) were measured by scanning a single nanoparticle in XY, XZ, or YZ dimensions with the individual laser beams alone or with both beams together. The laser light reflected from the nanoparticle was collected by the PMT detector in Channel 2, with the pinhole fully open (1 mm), and without any emission filter in the light path. Note that the intensity scales for the STED lasers in the PSF measurements (Figure 4) are $10^4 \sim 10^5$ times lower compared to that used for STED experiments (20~100 mW), while the intensity of the excitation laser for the PSF measurements was only 5~20 times less than that used for STED experiments (5 ~ 20 µW).

The temporal alignment between the excitation and the STED pulses on the specimen plane was verified by measuring the instrument response functions (IRF) for each laser and tuning the time delay between the two IRFs. The IRF was measured by recording the decay profile (TCSPC) or the phase histogram (FastFLIM) of the laser light reflected from the gold nanoparticles. The temporal tuning to optimize the pSTED performance was performed in two steps. First, a rough tuning was made by adjusting the length of the triggering cable between the master and the slave lasers so that the excitation IRF was immediately followed by the STED IRF. Fine tuning was achieved by adjusting the optical delay line (ODL in Figure 1) while observing the depletion effect at the same excitation and depletion laser powers each standard STED sample (e.g. fluorescent beads or Atto 647N dye solution) – the ODL was fixed when the best depletion was achieved.

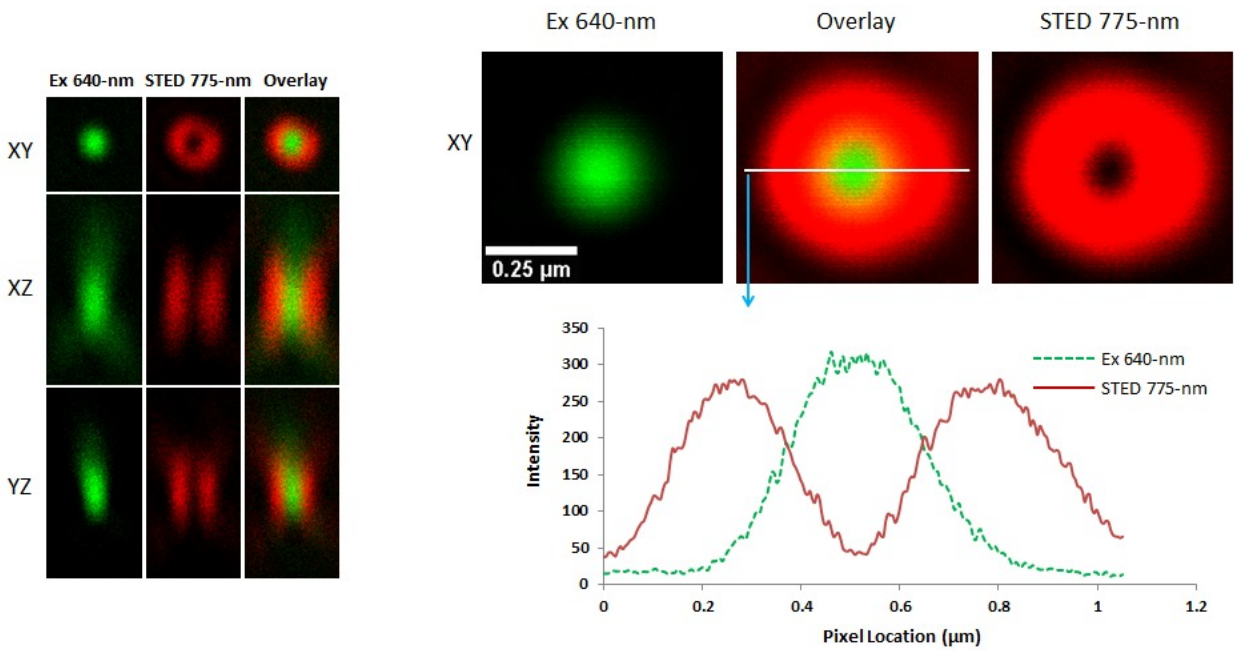

Figure 4: The spatial alignment of the excitation and STED laser beams.

3.2 The example pSTED images acquired by FastFLIM

Different samples were used to evaluate the performance of the pSTED using FastFLIM for data acquisition. Figure 5 compares images of the 60-nm fluorescent beads acquired by confocal and the pSTED. The pSTED clearly resolved the beads.

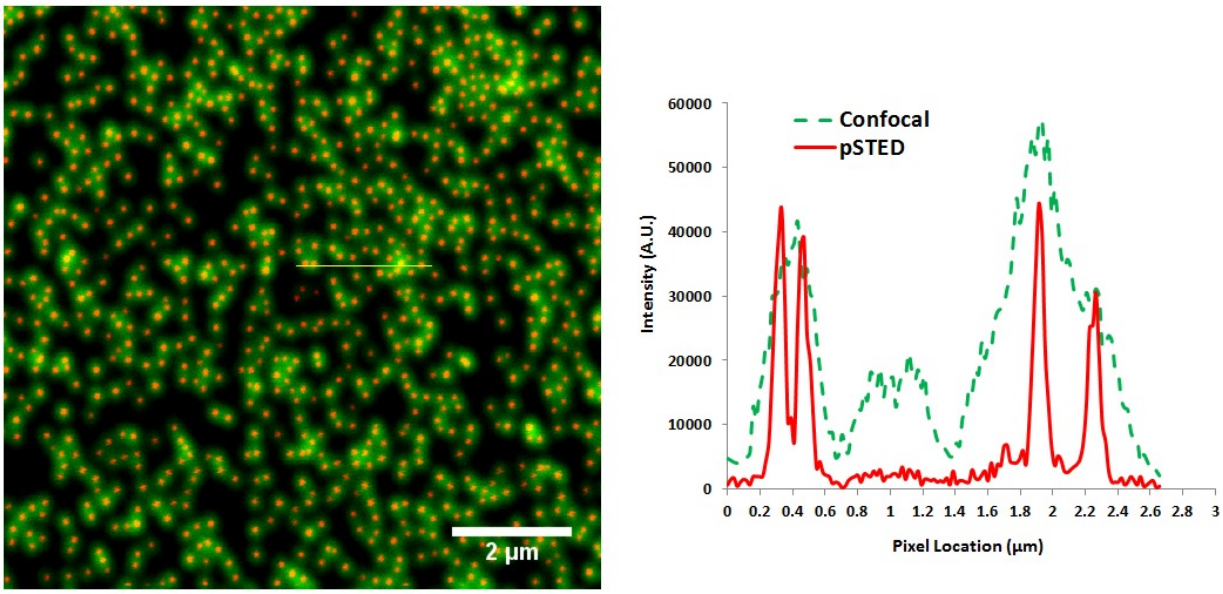

Figure 5: Confocal (green) vs. pSTED (red) images of 60-nm fluorescent beads, acquired by FastFLIM.

Figure 6 shows a comparison between the confocal and the pSTED images of the mitochondria membrane labeled with Atto 647N in fixed HeLa cells. The tubular structure of the mitochondria membrane, which cannot be seen in confocal, is clearly visualized by pSTED (inset).

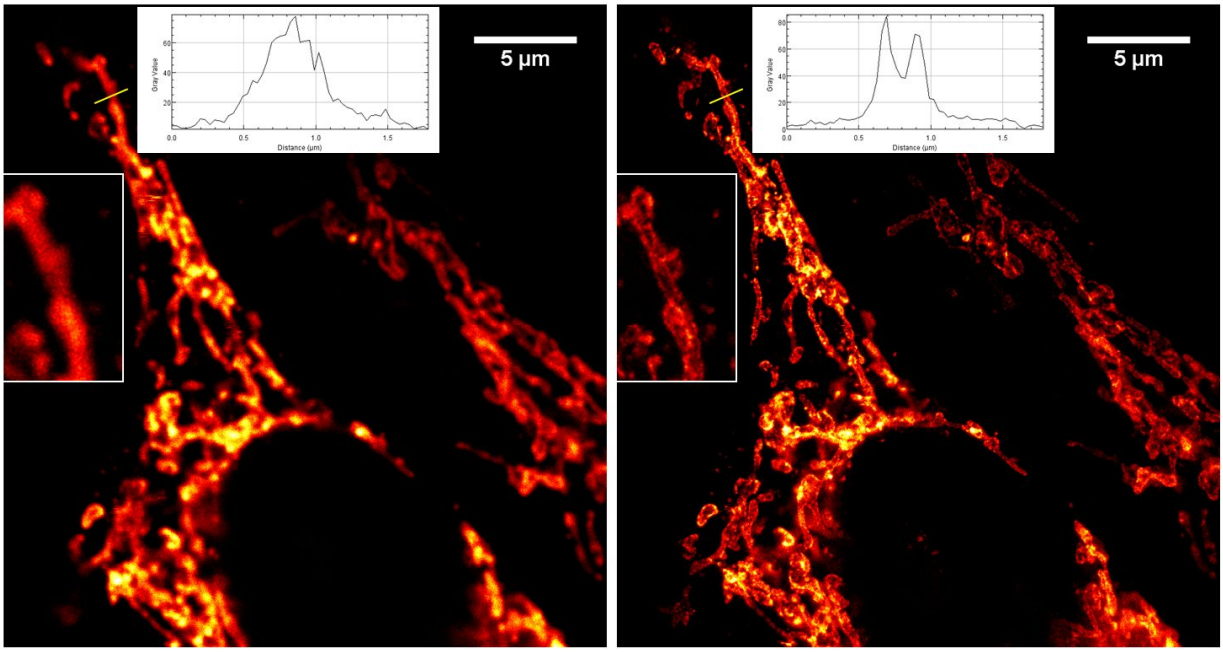

Figure 6: Confocal (left) vs. pSTED (right) images of the mitochondria membrane labeled with Atto 647N in fixed HeLa cells, acquired by FastFLIM.

Figure 7 shows a comparison between the confocal and the pSTED images of the mitochondria membrane labeled with Alexa Fluor 647 in live HeLa cells. At the ~30 mW STED power, the improvement in resolution is apparent, but we observed that there was substantial photo-bleaching, indicating that the Alexa Fluor 647 dye is probably not ideal for STED. In this regard, we observed negligible photo-bleaching at a much higher STED power (~50 mW) when using fixed HeLa cells labeled with Atto 647N.

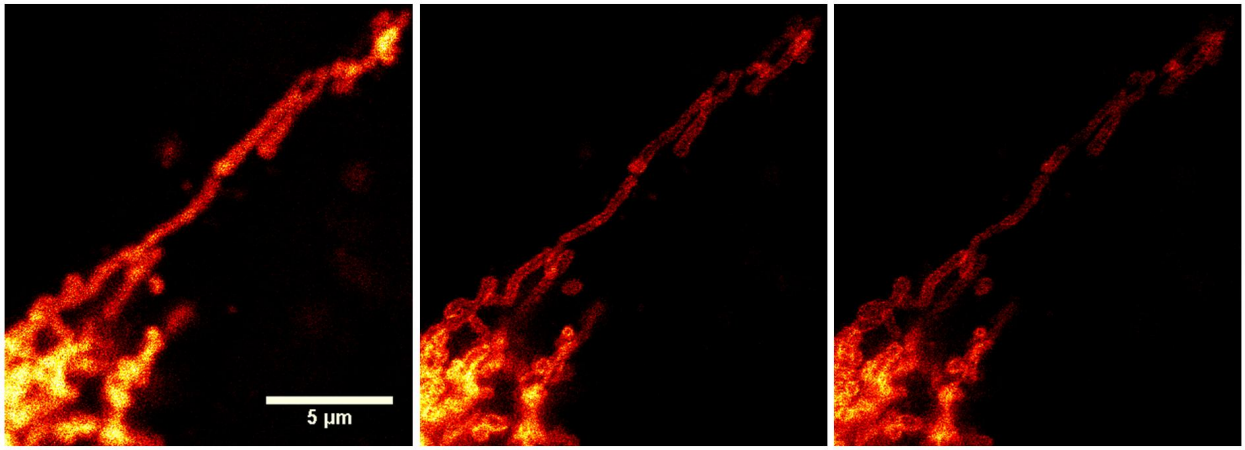

Figure 7: Confocal (left) vs. two time-point pSTED (middle and right) images of the mitochondria membrane labeled with Alexa Fluor 647 in live HeLa cells.

Another example of comparing the confocal vs. pSTED images is shown in Figure 8, by imaging the actin labeled with the SiR dye in fixed glia cells.

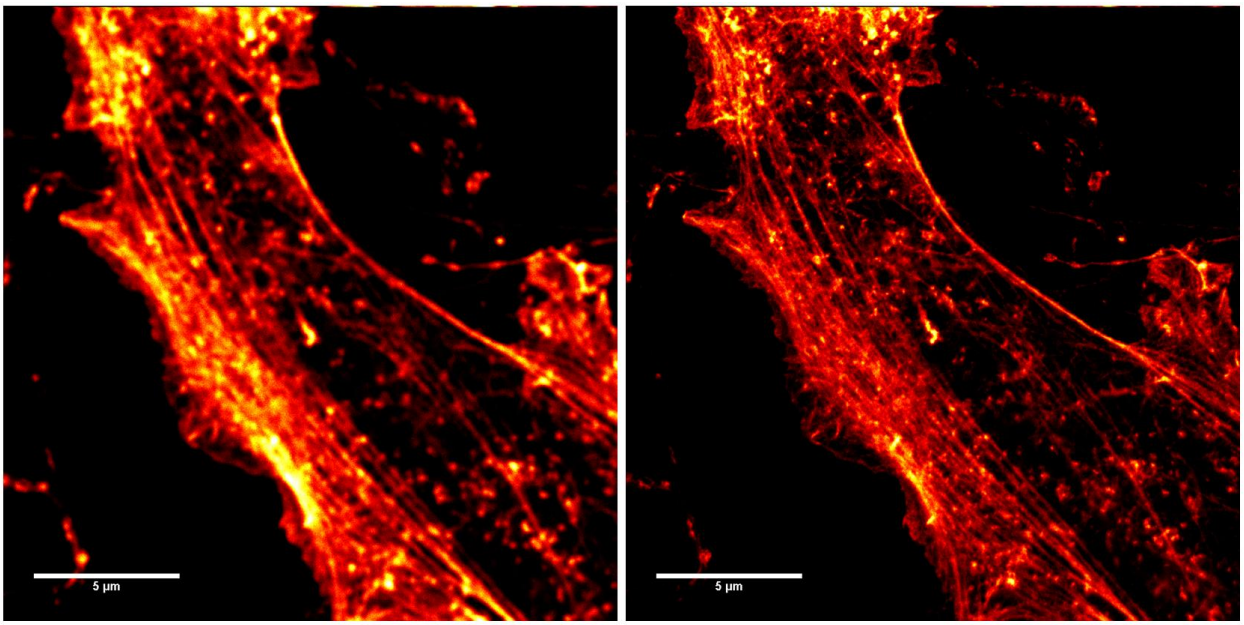

Figure 8: Confocal (left) vs. pSTED (right) images of the actin labeled with the SiR dye in fixed glia cells, acquired by FastFLIM.

To demonstrate the capability of using FastFLIM to acquire the time-resolved pSTED data to study molecule fast dynamics [31-33], we also carried out fluorescence lifetime correlation spectroscopy (FLCS) measurements in the time tagged time resolved (TTTR) mode. Figure 9 shows both the raw data traces and the calculated auto-correlation function (ACF) curves of the FLCS recordings of the Alexa 647 dyes in HPLC water, by using the pSTED beam only or the excitation beam only or both – the triplet effect was observed for the excitation only, but is not obvious when the pSTED beam was also applied given the same excitation power. In Figure 10, different ACF curves of the Atto 647N-goat anti-mouse-IgG antibodies (Activemotif Cat. #15058) in Phosphate-Buffered Saline (PBS) are compared for the excitation beam only vs. both excitation and the pSTED beams at different STED powers – as expected the higher the STED power, the smaller volume the excitation and the faster the diffusion time. The different decay dynamics obtained without and with STED are shown by the phasor plots, which were calibrated using a fluorescence lifetime standard Cy5 dissolved in HPLC water (0.95 ns).

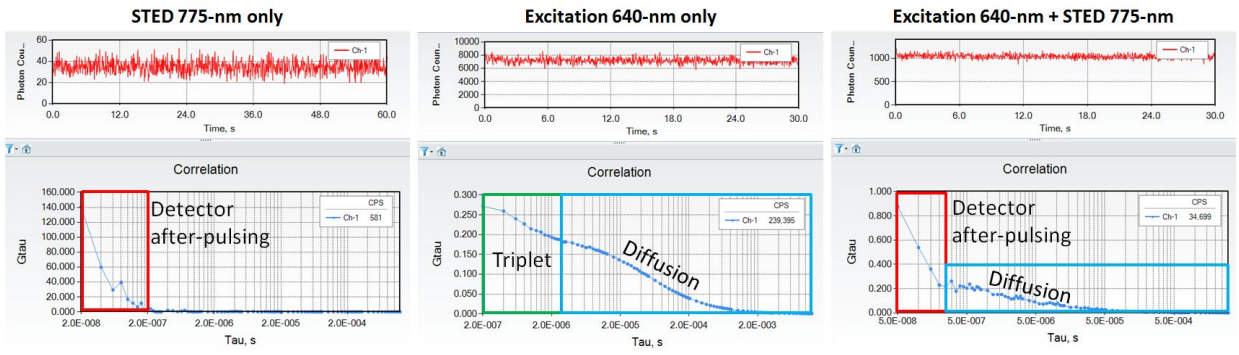

Figure 9: The pSTED FLCS of the Alexa Fluor 647 dyes in HPLC water.

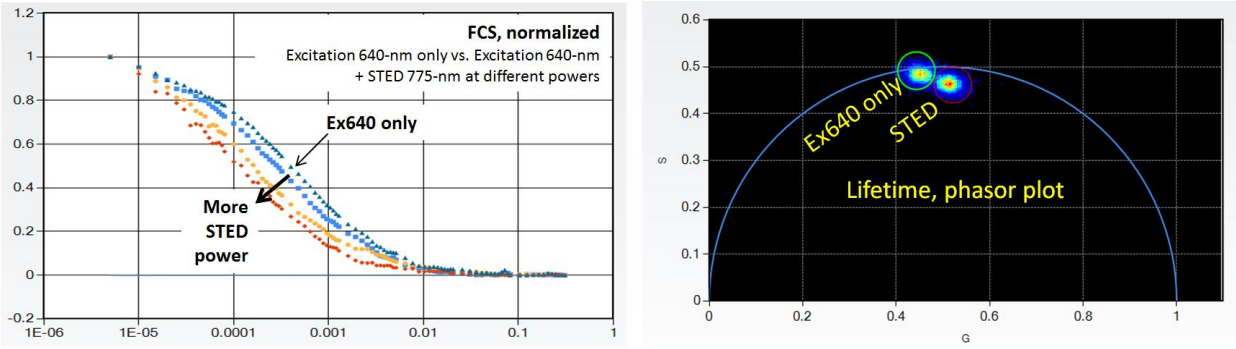

Figure 10: The pSTED FLCS of the Atto 647N-goat-anit-mouse-IgG antibodies in PBS.

3.3 The pSTED decay kinetics

To improve the resolution further we applied the phasor plot approach to the time-resolved data acquired by pSTED. Here, it is important to understand the pSTED decay kinetics. The fluorescence emission decay $I(t)$ in pSTED is governed by two exponential rates:

$$I(t) = kQe^{-kt}e^{-k_S\min(t,T)} = kQe^{-kt}e^{-\rho k[\min(t,T)]}$$

where k is the de-excitation rate and is equal to the reciprocal of the excited state lifetime (τ); Q is the fluorescence quantum yield; k_S is the stimulate emission decay rate; T is the pulse width of the depletion laser [13]. k_S is written as "ρk", where ρ is the saturation factor, defined by "I_{STED}/I_{Sat}" (described above). Assuming that the confocal PSF is simply determined by the radial (r) and the axial (z) beam waists, the time-dependent PSF – "$h(r, z, t)$" is thus given by

$$h(r,z,t) = e^{\left(-4\frac{r^2 z^2}{\omega^2\gamma^2}\right)}e^{-kt}e^{-\rho\frac{r^2}{\omega^2}k[\min(t,T)]}$$

where ω and γ are the radial and the axial beam waists, respectively [13]. Integrating the time-dependent PSF over space gives the pSTED decay kinetics:

$$I(t) = \frac{a[e^{-kt}+s]}{1+0.5\rho k[\min(t,T)]} + b$$

where ***a*** is the amplitude at time zero, ***s*** is the scatter noise at time zero, and ***b*** is the white noise background. This is similar to the cwSTED decay kinetics derived in the SPLIT method [14], except that a timing function "min(t, T)" characterizing the STED pusle is added.

Figure 11 shows the simulated pSTED decay kinetics with the following parameters: $a = 10^4$, $k = 0.33$ ($\tau = 3.33$ ns), $T = 600$ ps, $s = b = 0$, and $\rho = 10$ vs. 100. The similar decay kinetics were observed in the real pSTED measurements of 60-nm fluorescent beads, acquired by TCSPC (Figure 11). Since the decay kinetics are not affected after the STED pulse, the duration of the STED pulse relative to the fluorescence lifetime becomes an important factor for the effectiveness of the gating or the phasor plot approach. If the STED pulse is much shorter than the fluorescence lifetime, the gating or the phasor approach would become less effective. The STED pulse (~600 ps) used here is not quite narrow, providing an advantage of reducing the photo-toxicity compared to the very narrow pulse produced by stretching a Ti:Sapphire laser (< 200 ps); thus the gating or the phasor plot approach should be still very effective [18].

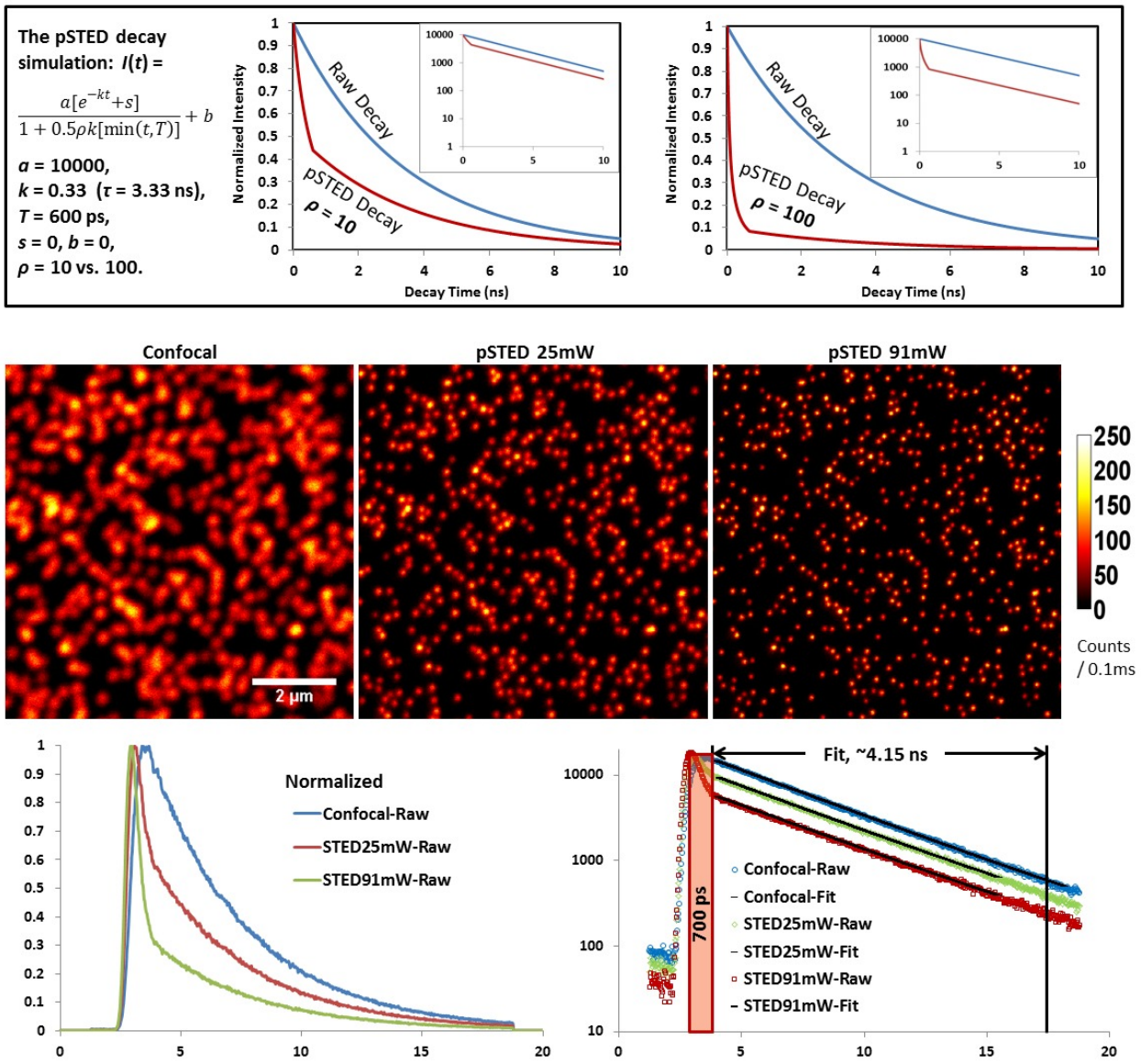

Figure 11: The pSTED decay kinetics.

3.4 Sharpening the pSTED image using a binary filter based on the phasor plot

In STED microscopy the same molecule can have different decay dynamics (species) upon its interaction with the excitation and the depletion laser beams, giving rise to two species: (A) the molecule will behave as a single- or multi-exponential decay when it is in the zero-depletion center of the donut and only excited, and (B) the decay will be distorted when the molecule is in the depletion region of the donut, where it is both excited and depleted. Together, these species (A and B) represent how the molecule spatially interacts with the excitation and the STED laser beams. While the signals of both species are collected, only the signals from species A are truly wanted and the signals from species B actually decrease the resolution.

By exploiting the time-resolved image acquisition by FastFLIM, we can separate species with different decay dynamics using the phasor plot approach, which was first used by the SPLIT method to increase the resolution of the time-resolved cwSTED image [14] (see Section 2.3). Since pSTED provides a better STED efficiency than cwSTED, the two species (A and B, discussed above) of the time-resolved pSTED image should be even better separated by the phasor plots. To

further sharpen the pSTED image acquired by FastFLIM, we then apply a simple binary filter to the image based on the phasor plots. This binary (1/0) filter idea is similar to the gating (on/off) concept. However, unlike the 1D gating function, which uses a simple cutoff between on and off along the decay time, the binary filter is actually a 2D function in the phasor space and is more precisely defined based on the decay kinetics of species A based on the phasor plots. This approach is simply given in three steps and can be implemented on-the-fly of the data acquisition by FastFLIM:

- First, establish the phasor distribution of specie A from the phasor plots of the confocal image acquired by using only the excitation laser – this reference should only need to be acquired once.
- Next, acquire the pSTED image(s).
- Finally, apply the binary filter to the pSTED image(s). For the pixels within the phasor distribution region of species A (established in the first step), the pixel intensity is multiplied by 1. For the rest of pixels (outside the phasor distribution region of species A), the pixel intensity is multiplied by 0.

Figure 12 illustrates the application of a binary filter based on the phasor plots to the pSTED image of fluorescent beads acquired by FastFLIM. From the confocal image acquired using only the excitation laser, the red cursor representing the phasor distribution of species A is defined. The same red cursor is then drawn on the phasor plots of the raw pSTED image. For the pixels within the red cursor, the pixel intensity is multiplied by 1, while the remaining pixel intensities are multiplied by 0. This yields the processed pSTED image with an improved resolution.

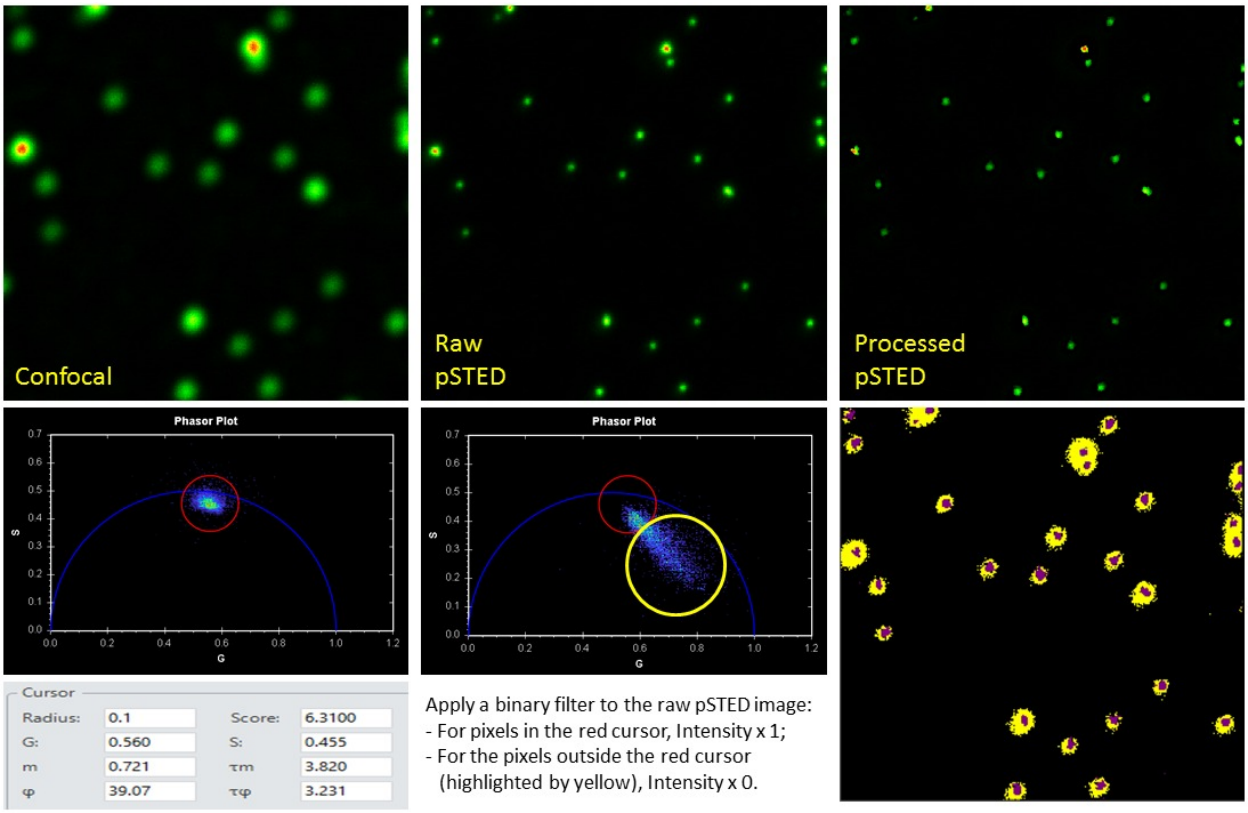

Figure 12: Sharpening the pSTED image using a binary filter based on the phasor plots.

3.5 Dual-label pSTED by FastFLIM using a single excitation/depletion beam combination

The multi-label STED microscopy imaging will undoubtedly help many applications by allowing the visualization of the finer details (e.g. below 50 nm) of different subcellular structures simultaneously. However, the imaging is also experimentally challenging, since it typically requires using different colored dyes, which may necessitate different combinations of excitation/depletion lasers. Using more than one STED laser can significantly increase the photo-

toxicity. On the other hand, most dyes for the best STED performance are still in the far red spectrum – it would be advantageous to acquire STED images of using two different dyes in the same far red spectrum

We demonstrate a new way of the dual-label pSTED imaging by FastFLIM, using a single excitation / depletion laser combination. The two dyes should have similar absorption-emission spectra, and thus can be optimally excited by the same excitation laser wavelength and efficiently depleted by the same STED laser wavelength; a specific requirement is that both dyes need to have distinct fluorescence lifetimes (ideally at least 1-ns difference). The time-resolved pSTED image of the dual labels is acquired by FastFLIM in the same way as for the single label. The two labels are then differentiated from the phasor plots of the time-resolved pSTED image, resulting in two separate pSTED images representing the two labels, respectively. Finally, the two pSTED images assigned with two different false colors are merged.

As a proof of the concept, Figure 13 demonstates the dual-label (Atto 647N and Atto 655) pSTED image acquired by FastFLIM. The two dyes are first separated from the phasor plots, and then assigned with two different false colors (Atto 647N – yellow, Atto 655 - purple) to produce the processed and merged pSTED image of the two labels.

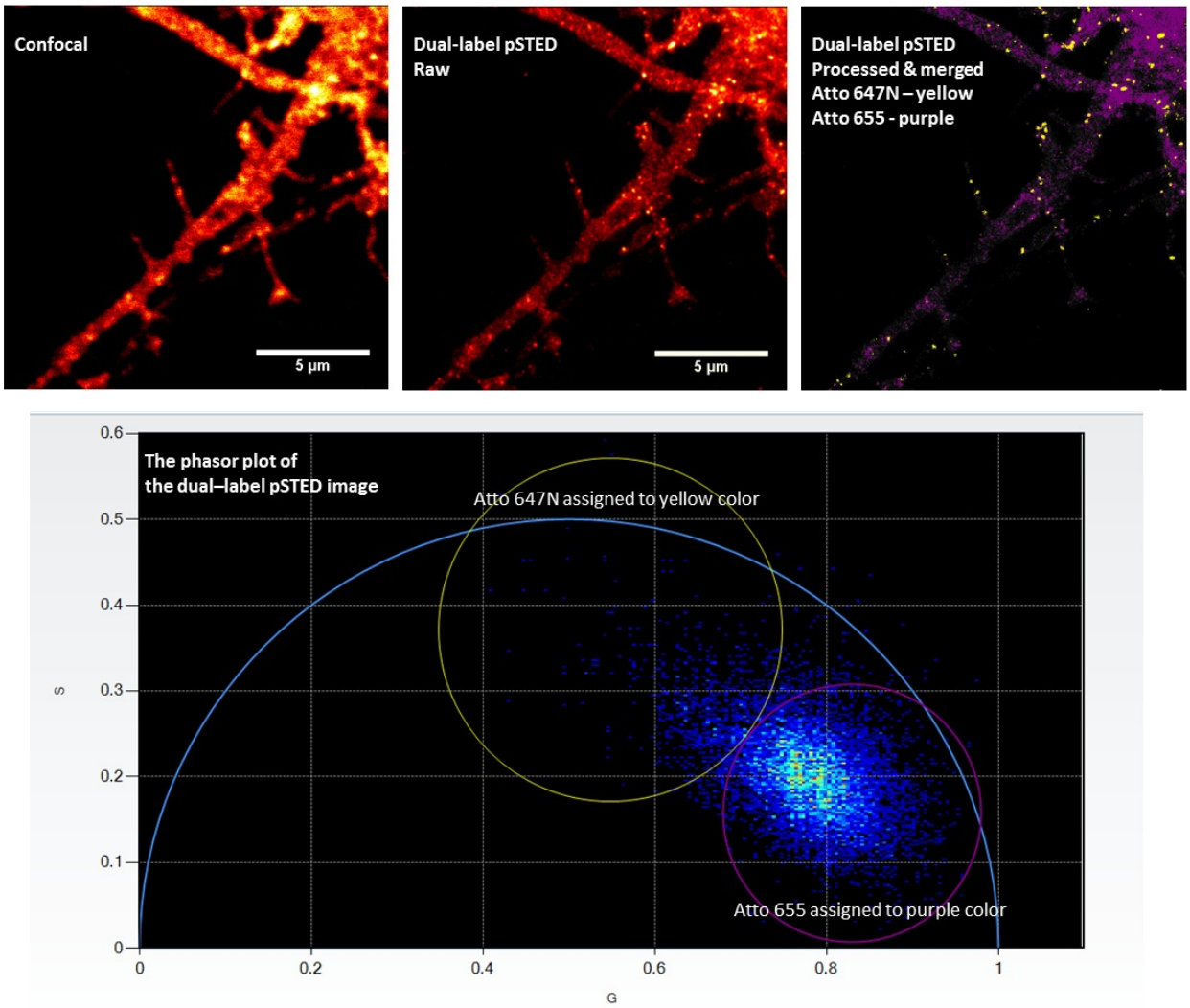

Figure 13: Dual-label pSTED by FastFLIM using a single excitation / depletion laser combination.

4. CONCLUSION

We present a novel pSTED method using FastFLIM for the time-resolved acquisition of STED data, and demonstrate its capability for different STED microscopy measurements. Compared to the classical TCSPC method of high temporal-resolution, we show that the FastFLIM approach can tolerate a much higher photon counting rate, and thus provide a large dynamic range for quantitative STED measurements. Importantly, the FastFLIM approach accurately measures the complicated decay kinetics over a wide range of lifetimes. We show that the time-resolved pSTED images acquired by FastFLIM can be sharpened by applying a binary filter based on the phasor plots. We also show that the combination of FastFLIM and the phasor plot is a promising approach for dual-label STED measurements using a single excitation/STED combination, and has the potential to drive STED microscopy into new dimensions.

REFERENCE

[1]. S. W. Hell and J. Wichmann. Breaking the di□raction resolution limit by stimulated emission: stimulated-emission-depletion fluorescence microscopy. Optical Letters, 19(11), 780–782 (1994).
[2]. S.W. Hell. Far-field optical nanoscopy. Science 316(5828), 1153–1158 (2007).
[3]. S.W. Hell, Microscopy and its focal switch. Nature Methods 6(1), 24-32 (2009).
[4]. E. Betzig, G.H. Patterson, R. Sougrat, O.W. Lindwasser, S. Olenych, J.S. Bonifacino, M.W. Davidson, J. Lippincott-Schwartz and H.F. Hess. Imaging intracellular fluorescent proteins at nanometer resolution. Science. 313:1642–1645 (2006).
[5]. S.T. Hess, T.P. Girirajan and M.D. Mason. Ultra-high resolution imaging by fluorescence photoactivation localization microscopy. Biophys. J. 91:4258–4272 (2006).
[6]. M.F. Juette, T.J. Gould, M.D. Lessard, M.J. Mlodzianoski, B.S. Nagpure, B.T. Bennett, S.T. Hess, and J. Bewersdorf. Three-dimensional sub-100nm resolution fluorescence microscopy of thick samples. Nat. Methods. 5:527–529 (2008).
[7]. G. Patterson, M. Davidson, S. Manley and J. Lippincott-Schwartz. Superresolution imaging using single-molecule localization. Annu. Rev. Phys. Chem. 61, 345–367 (2010).
[8]. B. Huang, S.A. Jones, B. Brandenburg and X. Zhuang. Whole-cell 3D STORM reveals interactions between cellular structures with nanometerscale resolution. Nat. Methods. 5:1047–1052 (2008a).
[9]. B. Huang, W. Wang, M. Bates and X. Zhuang. Three-dimensional super-resolution imaging by stochastic optical reconstruction microscopy. Science. 319:810–813 (2008b).
[10]. B. Huang, M. Bates and X. Zhuang. Super-resolution fluorescence microscopy. Annu. Rev. Biochem. 78, 993–1016 (2009).
[11]. S.W. Hell, S. Sahl, X. Zhuang, R. Heintzmann, M. Booth, J. Bewersdorf, G. Shtengel, H. Hess, P. Tinnefeld, A. Honigmann, S. Jakobs, I. Testa, L. Cognet, B. Lounis, H. Ewers, S. Davis, D. Klenerman, K. Willig, G. Vicidomini , M. Castello, A. Diaspro, T. Cordes, M. Bates and C. Eggeling. The 2015 Super-Resolution Microscopy Roadmap. J Phys D: Appl Phys, 48, 443001 (2015).
[12]. Vicidomini, G., Moneron, G., Han, K. Y., Westphal, V., Ta, H., Reuss, M., ... Hell, S. W. Sharper low-power STED nanoscopy by time gating. Nature Methods, 8(7), 571–573 (2011).
[13]. Vicidomini, G., Schönle, A., Ta, H., Han, K. Y., Moneron, G., Eggeling, C., & Hell, S. W. STED nanoscopy with time-gated detection: Theoretical and experimental aspects. PLoS ONE, 8(1), e54421 (2013).
[14]. L. Lanzano, I. C. Hernandez, M. Castello, E. Gratton, A. Diaspro and G. Vicidomini. Encoding and decoding spatio-temporal information for super-resolution microscopy. Nature Communications 6(6701), 1-9 (2015).
[15]. Klar, T. A. and S. W. Hell. Subdiffraction resolution in far-field fluorescence microscopy. Optics Letters. 24 (14): 954–956 (1999).
[16]. Dyba, M., & Hell, S. W. (2003). Photostability of a fluorescent marker under pulsed excited-state depletion through stimulated Emission. Applied Optics, 42(25), 5123–5129
[17]. Bianchini, P., Peres, C., Oneto, M., Galiani, S., Vicidomini, G., & Diaspro, A. (2015). STED nanoscopy: A glimpse into the future. Cell and Tissue Research, 360(1), 143–150.
[18]. Castello M, Tortarolo G, Hernández IC, Bianchini P, Buttafava M, Boso G, Tosi A, Diaspro A, Vicidomini G. Gated-sted microscopy with subnanosecond pulsed fiber laser for reducing photobleaching. MRT 79(9): 785-91 (2016).
[19]. Colyer, R.A., Lee, C. & Gratton, E. A novel fluorescence lifetime imaging system that optimizes photon efficiency. *Microsc. Res. Tech.* 71, 201–213 (2008).
[20]. W. Becker. The Bh TCSPC Handbook 5th Edition. (2012); page 76.
[21]. Digman, M. A., V.R. Caiolfa, M. Zamai and E. Gratton. The phasor approach to fluorescence lifetime imaging analysis. Biophys. J. 94, L14-6 (2008).
[22]. Stringari, C., A. Cinquin, O. Cinquin, M.A. Digman, P.J. Donovan and E. Gratton. Phasor approach to fluorescence lifetime microscopy distinguishes different metabolic states of germ cells in a live tissue. Proc. Natl. Acad. Sci. U. S. A. 108, 13582-13587 (2011).
[23]. Redford, G. I. and R.M. Clegg. Polar plot representation for frequency-domain analysis of fluorescence lifetimes. J. Fluoresc. 15, 805-815 (2005).
[24]. Hanley, Q. S. and A.H. Clayton. AB-plot assisted determination of fluorophore mixtures in a fluorescence lifetime microscope using spectra or quenchers. J. Microsc. 218, 62-67 (2005).

[25]. Clayton, A. H., Q.S. Hanley and P.J. Verveer. Graphical representation and multicomponent analysis of single-frequency fluorescence lifetime imaging microscopy data. J. Microsc. 213, 1-5 (2004).
[26]. S.-C. Liao, Y. Sun and U. Coskun. FLIM Analysis using the Phasor Plots. http://www.iss.com/resources/pdf/technotes/FLIM_Using_Phasor_Plots.pdf
[27]. Y. Sun and S.-C. Liao. The Ultimate Phasor Plot and beyond. http://www.iss.com/resources/pdf/appnotes/Phasor_Plot_And_Beyond.pdf
[28]. Ballister ER, Ayloo S, Chenoweth DM, Lampson MA, Holzbaur ELF. Optogenetic control of organelle transport using a photocaged chemical inducer of dimerization. Curr Biol. 2015 May 18;25(10):R407–8.
[29]. Teng KW, Ishitsuka Y, Ren P, Youn Y, Deng X, Ge P, Belmont AS, Selvin PR. Labeling proteins inside living cells using external fluorophores for microscopy. eLife. 2016 Dec 9;5:e20378.
[30]. Cai, E., Ge, P., Lee, S. H., Jeyifous, O., Wang, Y., Liu, Y., Wilson, K. M., Lim, S. J., Baird, M. A., Stone, J. E., Lee, K. Y., Davidson, M. W., Chung, H. J., Schulten, K., Smith, A. M., Green, W. N. and Selvin, P. R. (2014), Stable Small Quantum Dots for Synaptic Receptor Tracking on Live Neurons. Angew. Chem. Int. Ed., 53: 12484–12488.
[31]. L. Kastrup, H. Blom, C. Eggeling and S.W. Hell. Fluorescence Fluctuation Spectroscopy in Subdiffraction Focal Volumes. Phys. Rev. Lett. 94, 178104 (2005).
[32]. C. Eggeling, C. Ringemann, R. Medda, G. Schwarzmann, K. Sandhoff, S. Polyakova, V.N. Belov, B. Hein, C. von Middendorff, A. Schönle and S.W. Hell. Direct observation of the nanoscale dynamics of membrane lipids in a living cell. Nature, 457(7233), 1159–1162 (2009).
[33]. Vicidomini G, Ta H, Honigmann A, et al. STED-FLCS: An Advanced Tool to Reveal Spatiotemporal Heterogeneity of Molecular Membrane Dynamics. *Nano Letters*.15(9):5912-5918 (2015).